# Microfluidic Single-Cell Monitoring Versus Microplate Bulk-Cell Measurement

Abolfazl Rahimi , Sapna Kannan , XiuJun Li , Paul Chi Hang Li *

Posted Date: 20 November 2025

doi: 10.20944/preprints202511.1437.v1

Keywords: cell fluorescence; lung cancer cells; ACE2-enriched A549 cells; microfluidic chip; microplate reader

 doi:10.20944/preprints202511.1437.v1



*Article*

# Microfluidic Single-Cell Monitoring Versus Microplate Bulk-Cell Measurement

**Abolfazl Rahimi [1], Sapna Kannan [2], XiuJun Li [2] and Paul C. H. Li [1,*]**

[1] Department of Chemistry, Simon Fraser University, Burnaby, BC, Canada V5A 1S6

[2] Department of Chemistry and Biochemistry, Forensic Science, & Border Biomedical Research Center, University of Texas at El Paso, El Paso, TX 79968, USA

* Correspondence: paulli@sfu.ca; Tel.: (+1)-778-782-5956

**Abstract**

This study compares two methods for measuring cell changes: a microfluidic chip single-cell monitoring and a microplate bulk-cell measurement. As intracellular calcium ion concentration ([Ca2+]i) plays a critical role in various cellular functions and biochemical processes, measurements of [Ca2+]i may be used to compare the two methods. The microfluidic approach allows real-time monitoring of individual cells, utilizing the fluorescence emitted from calcium-Fluo 4 chelate, while the microplate method offers bulk analysis of approximately 10,000 cells per well in a 96-well microplate. We have demonstrated that the single-cell method provides insights into [Ca2+]i dynamics with low reagent consumption and rapid analysis, whereas the microplate method enables comprehensive bulk measurements when isolation of single cells is difficult. By integrating both techniques, we aim to complement measurements on both single-cell and population levels, especially when cell availability is an issue. For the cellular process, we specifically investigated the increase in [Ca2+]i following histamine receptor activation, in ACE2-enriched A549 and wild-type A549 cells. In our findings, both approaches yielded consistent calcium-signaling patterns, that wild-type A549 cells exhibited stronger histamine-induced calcium responses than ACE2-enriched cells, and that the two methods complement each other—single-cell assays providing temporal and low-reagent analysis, while bulk assays provide high-throughput, population-level averages.

**Keywords:** cell fluorescence; lung cancer cells; ACE2-enriched A549 cells; microfluidic chip; microplate reader

## 1. Introduction

Many methods for measuring cell changes have been developed, and these include bulk-cell measurements conducted with microplates [1], flow cytometry [2,3], and cell imaging [4]. On the other hand, single-cell monitoring has been achieved on different single cells using flow cytometry [2,3], and on the same single cells by the microfluidic chip [5–7]. While the microfluidic chips have been used to provide real-time changes monitored on the same single cells, there are concerns about the type of information obtained in measuring only a limited amount of single cells [8–10]. So, a knowledge gap exists that the limitations of the microfluidic method may be unclearly founded in the light of the merits of the bulk-cell method. Therefore, in this study, the two methods are directly compared, and the comparison was made using a well-established cell assay: the cell calcium assay. In order to implement the assay for direct comparison, the stimulant or drug for the assay should be selected, and so is the type of cells that is to be chosen.

In cell biology, intracellular calcium plays pivotal role as a universal second messenger that regulates a vast range of cellular functions. For example, the increase of cytosolic $Ca^{2+}$ concentration or $[Ca^{2+}]_i$ is associated with the activation of G-protein-coupled receptors (GPCRs) which are considered the drug targets of 50-60% of therapeutic agents [11,12]. Consequently, measuring cytosolic calcium is a crucial assay to be selected for our comparison study. Many microfluidic studies

 doi:10.20944/preprints202511.1437.v1



have been conducted using different human cell types, e.g., muscle [13,14], osteoblast [15], glioma [6,16], endothelial [17], intestinal [18,19], kidney [20], tumor microtubes [21], and others such as CHO cells [22].

A549 cells, which belong to a type of lung cancer cell [23], have also been studied for cell calcium. A549 cells express H1 and H2 histamine receptors and their responses to histamine to produce the increase in cytosolic calcium concentration has been previously studied [25,40]. The measurement of the increase in cytosolic calcium concentration can be achieved by using a fluorescent calcium indicator dyes, such as Fura-2 or Fluo-4 [24–27].

Therefore, we selected to use A549 cells for the cell assay and chose the cell stimulant to be histamine. Since all these previous studies using microplates and flow cytometry were not performed at the single-cell scale, direct comparison is not straightforward. This study is novel in that it directly compares bulk-cell and single-cell calcium measurements performed under identical experimental conditions.

## 2. Materials and Methods

### *2.1. Reagents*

The reagents used consist of DMSO (99.9%), DMEM/high-glucose medium (supplemented with sodium pyruvate, 10% fetal bovine serum (FBS), and 1% penicillin, Hanks' balanced salt solution (HBSS), phosphate-buffered saline (PBS), 0.05% trypsin-EDTA and ionomycin.

The increase in $[Ca^{2+}]_i$ in mammalian cells has been evaluated using fluorescent calcium indicator dyes, such as Fura 2 [1,28], or Fluo 4 [29]. Here, the probe Fluo 4 AM ester (50 μg, special packaging) was used. It was first dissolved in 50 μL DMSO to prepare a 1 mg/mL stock solution. Since the fluorescence probe is a light-sensitive dye, it must be stored in dark at -20 °C. Before use, the stock solution was freshly diluted in HBSS to make a 5.0 μM working solution. Trypan blue solution (0.4%) was used to evaluate the viability of the cell under the microscope.

Histamine, which is endogenous in humans and released to other tissues upon stimulation by an allergen or other irritants [30–35], is also available commercially. Histamine dihydrochloride (98%) was obtained from Thermo Scientific Chemicals; a stock solution of 100 μM was prepared by dissolving the compound in deionized water. This stock solution was subsequently diluted in HBSS to create working solutions of 5 μM and 10 μM.

### *2.2. Cell Culture*

A549 is a line of wild-type human alveolar epithelial cells. A549-hACE2 cell line, which is a commonly used cellular model for the study of respiratory infections, has been generated from the A549 lung carcinoma cell line [36]. A549-hACE2 cells were stably transfected to express the human ACE2 (hACE2) gene. In contrast to their parental cell line, A549-hACE2 cells are permissive to infection by SARS-CoV-2 and/or spike-pseudotyped lentiviral particles. Accordingly, the cells are ideal for studying the SARS-CoV-2 Spike protein, viral entry into host cells, as well as for screening small molecule inhibitors and neutralizing antibodies.

Briefly, the frozen cell vial was thawed by gentle agitation in a 37 °C water bath. To reduce the possibility of contamination, the vial's cap and O-ring were kept out of water. Thawing should be rapid (approximately 2 minutes). Then, the vial was removed from the water bath as soon as the contents are thawed, and the vial was decontaminated by dipping in, or spraying with, 70% ethanol. After the cap was removed, the cells were transferred to a larger tube containing 15 mL of pre-warmed growth medium. Selection antibiotics was not added until the cells have been passaged twice.

Using a centrifuge (Eppendorf 5804), the tube was spun at 1400 rpm for 5 min using a rotor (F34-6-38, 11.5 cm radius) with a g-force of 252 g. The supernatant containing the cryoprotective agent was removed and cells were resuspended with 1 mL of growth medium. The contents were transferred to a T-25 tissue culture flask containing 5 mL of growth medium without selective antibiotics. The

 doi:10.20944/preprints202511.1437.v1



culture was incubated at 37 °C in 5% $CO_2$. The confluency of the cells was monitored according to Figure 1.

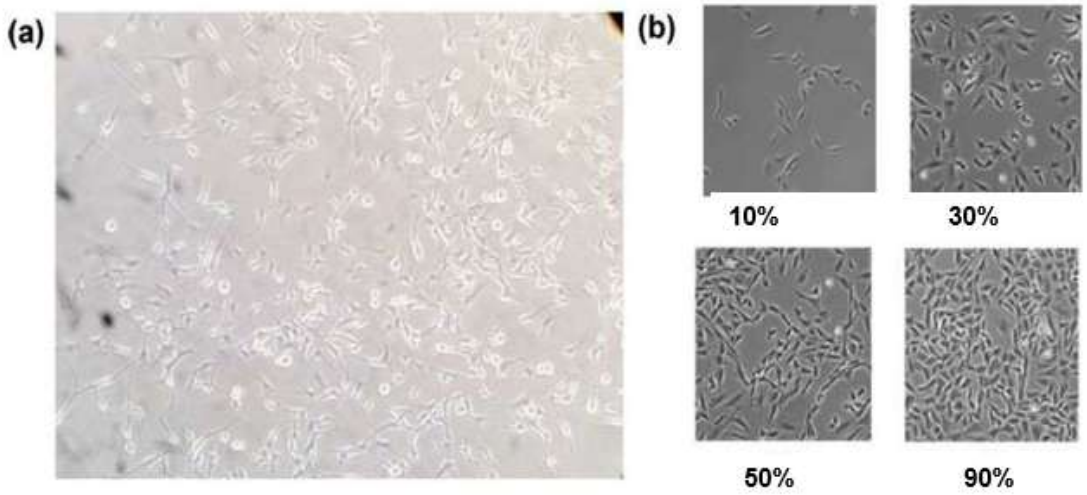


**Figure 1.** Culture of A549 cells. (a) adherent A549 cells (star-shaped) and detached cells (round), (b) guide of estimated percent of confluency (10, 30, 50, 90%). The cell size of ~20 μm.

*2.3. Single Cell Assay Using the Microfluidic Chip*

To conduct single cell assay, a glass chip that consisted of three reservoirs, three channels, and one chamber was employed (Figure 2a), as previously reported [6]. The fabrication of the glass chip was previously reported [29,37]. This chip was comprised of a chamber and a V-shaped cell retention structure for single-cell isolation; whereas Reservoir 2 was used for drug delivery. The channel was 40 μm deep, while the reservoirs (2.5 mm in diameter) were 0.6 mm deep [6].

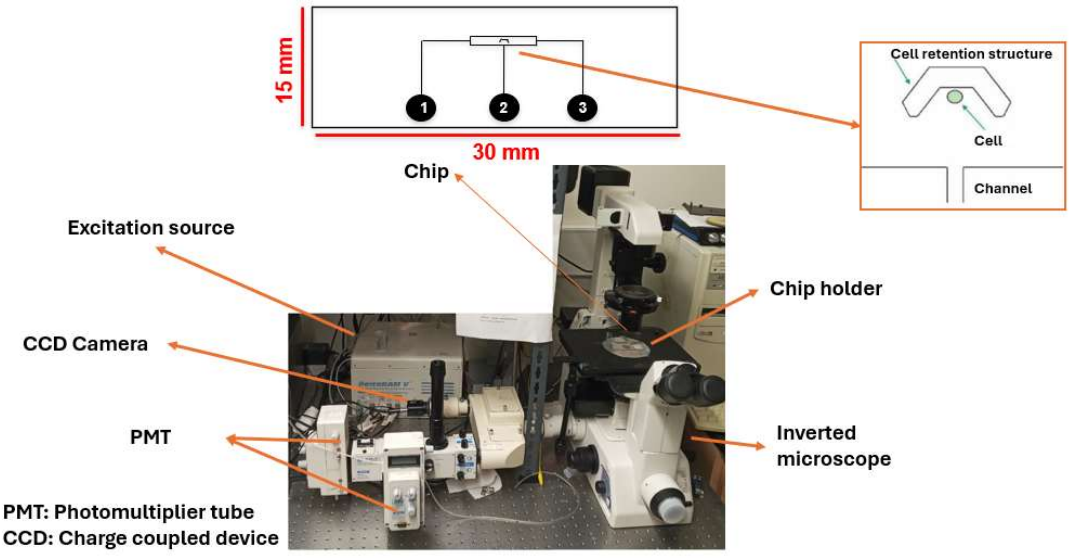


**Figure 2.** The microfluidic chip and the optical imaging/ fluorescence measurement system. An image of the instrument setup consisting of an inverted microscope, chip holder, photoexcitation source, CCD camera, and PMT [3]. Top inset: The schematic diagram of the microfluidic chip consisting of three solution reservoirs (Reservoirs 1, 2, 3) and cell retention structure located within the chamber connected with three microchannels.

 doi:10.20944/preprints202511.1437.v1



Right inset: A single cell is retained in the cell retention structure that is opposite to the reagent channel (90 μm wide) leading to Reservoir 2.

An optical system with an inverted microscope (TE300, Nikon) and a CCD camera was used for bright-field imaging, see Figure 2b. For easy and clear microscopic observation, a TV monitor was used, with a video capture card installed in a computer for image capture according to Figure 2.

Cell introduction and selection were conducted after the chip was washed, as previously reported [16]. Briefly, the cell medium from Reservoir 1 was removed as much as possible (Figure 3). Then, the cell suspension was resuspended gently and a small aliquot (5 μL) was added into Reservoir 1. When a small amount of medium was removed from Reservoir 3, the cell should move from left to right (Figure 3). When the cell moved closer to the entrance of the cell retention structure, some cell medium was added to the right (Reservoir 3). In this manner, the liquid pressure difference was established, and a desired cancer cell would be moved and stabilized in position within or near the cell retention structure.

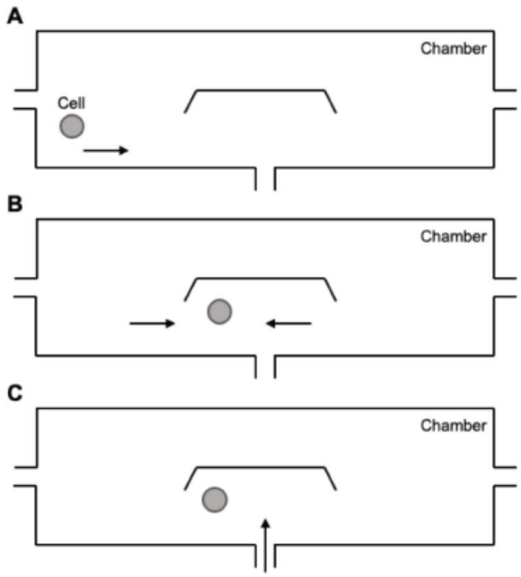


**Figure 3.** Schematic diagrams displaying how a single cell is selected and retained in the cell retention structure. (A) Cell suspension was introduced through Reservoir 1 flowing from the left side of the chamber. (B) the liquid level of Reservoir 1 and 3 was adjusted to make the cell stop near the cell retention structure in the middle of the chamber. (C) Upon cell retention, any chemical reagents were administrated through Reservoir 2 that is directly opposite the cell retention structure, see Figure 2 right inset.

Single-cell intracellular calcium measurement was performed on this fluorescence microscope platform following a previously published procedure from our group [1,14]. Using the fluorescence intensities obtained from the microfluidic method, the change in cell calcium concentration, $[Ca^{2+}]_i$ can be calculated using equation 1:

$$[\mathrm{Ca}^{2+}]_i = K_\mathrm{d} \frac{F - F_\mathrm{min}}{F_\mathrm{max} - F}$$

where $F$ shows measured fluorescence; $K_d$ represents the dissociation constant of Fluo-4 $Ca^{2+}$ complex and has a value of 0.35 μM [38]; $F_{min}$ is the background fluorescence intensity (in the calcium-free surrounding solution); $F_{max}$ indicates maximum fluorescence induced by ionomycin that facilitates calcium entry through the cell membrane to saturate the Fluo 4 dye in the cell.

*2.4. Bulk Cell Analysis Using the Microplate Reader*

 doi:10.20944/preprints202511.1437.v1



A black clear-bottom cell-culture grade COC-coated 96-well plate (model 3880, Corning NY USA) was used. Wells A1-6, B1-6, C1-6 and D1 were used, see Figure 4. The wells are seeded with A549 cells (A1 to C3) and ACE2-enriched A549 cells (A4-C6) at a density of 10,000 cells per well. Cells were counted using a hemocytometer. Experiments in triplicate (A, B, C) were caried out at 24 h after cell seeding to ensure cell adherence to the well bottoms and desired cell confluency.

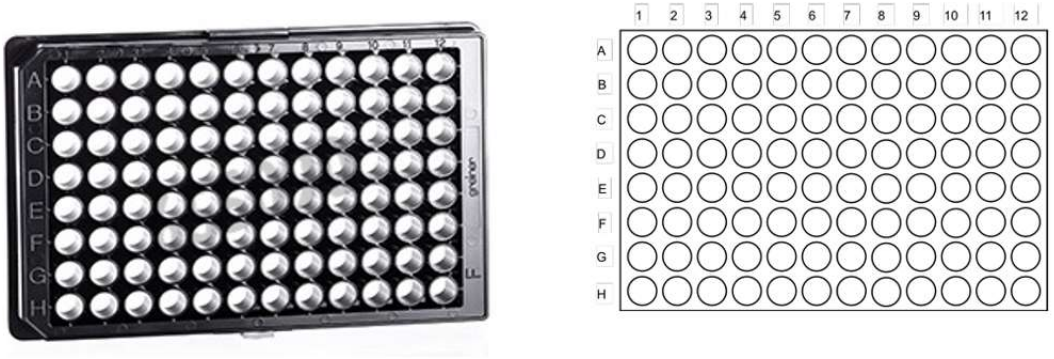


**Figure 4.** Image and schematic diagram of the 96-well culture microplate. The plate is black clear-bottom for fluorescence measurements on the cell adhered to the well bottoms. The wells are arranged in eight rows (A-H) and 12 columns (1-12).

To load the calcium dye Fluo-4, cells in wells (A1-6, B1-6, C1-6) were treated with freshly prepared 5 μM Fluo-4 AM working solutions and incubated for 45 min at 37° C. After incubation, the extracellular dye solution was removed and wells were washed and then topped up with HBSS. The total volume per each well was 200 μL. Using a Tecan M200 plate reader (Tecan, Switzerland), first measurements were made to all wells (in the bottom reading mode) to establish the baseline. A cell-free well (D1) was also measured to establish $F_{min}$, see equation 1.

Then, the cells in each well were treated with different concentrations of histamine, i.e., 1 μM (1A-C and 4A-C), 5 μM (2A-C and 5A-C), 10 μM (3A-C and 6A-C). Measurements were performed with the M200 plate reader. The temperature inside the plate reader was maintained at 37° C throughout the experiments to mimic physiological conditions. The following settings were used on the Tecan iControl software for measurements: fluorescence bottom reading (which is a more sensitive mode for adherent cells compared to top reading mode), 470 nm excitation wavelength, 530 nm emission wavelength, 25 flashes, 20 μs integration, 0 μs lag time, 0 μs settle time.

Using the fluorescence intensities obtained, i.e., $F_{min}$, $F$ and $F_{max}$, the change in cell calcium concentration, $[Ca^{2+}]_i$ can be calculated using equation 1, where $F$ shows the average of the measured fluorescence (three-replicates or n = 3); $F_{min}$ is the background fluorescence intensity (in the calcium-free well); $F_{max}$ indicates maximum fluorescence induced by ionomycin added to the cell in the wells.

## 3. Results and Discussion

Figure 5 illustrates the change in the fluorescent intensity due to histamine as measured in a single-cell of wild type A549. The changes occurred after dye loading (1, 2, 3) but before ionomycin treatment (4). It is because histamine can interact with the cells via histamine receptors [39,40]. All the histamine receptors are subtypes of GPCRs which will produce cytosolic calcium increase upon activation [3,41–43].

 doi:10.20944/preprints202511.1437.v1



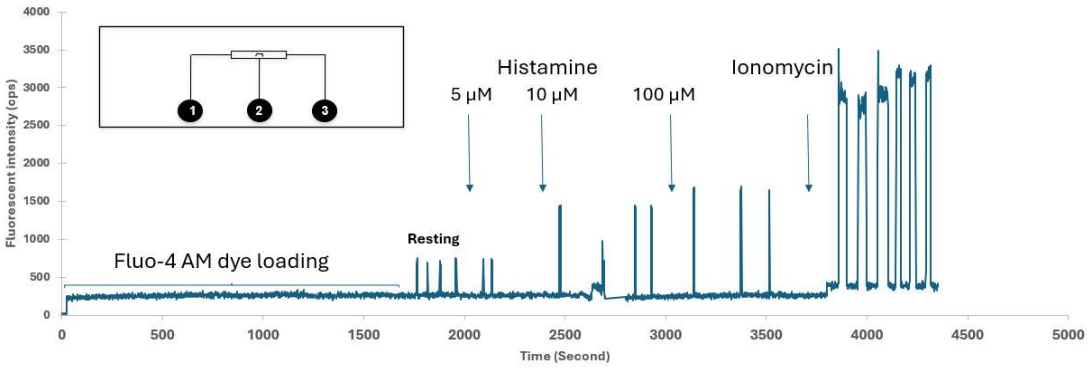


**Figure 5.** Change in fluorescence intensity (in counts per second or cps) due to cytosolic calcium measured by single-cell analysis. The baseline represented the background level when the cell was out of the measurement window; whereas the peaks depicted the cell signals (over the background) when the cell fluorescence was measured. The single wild-type A549 cell was stimulated with different concentrations of histamine (5, 10, 100 μM), followed by ionomycin treatment as various time points indicated by 1, 2, 3, 4, respectively. The initial region indicated low fluorescence when Fluo 4 AM dye was loaded into the cell with low and resting calcium level before reagent stimulation.

The variations in intensities in the fluorescence measurements were converted to calcium concentrations using equation 1. The average of three experiments is shown in Figure 6 (blue columns). It is seen that the cytosolic calcium concentration of the wild type A549 cell is low at rest (i.e., before reagent stimulation) but it increases after the addition of histamine. The increase of cytosolic calcium in A549 cells is greater when the histamine concentrations are raised from 5 μM to 10 μM, and finally to 100 μM.

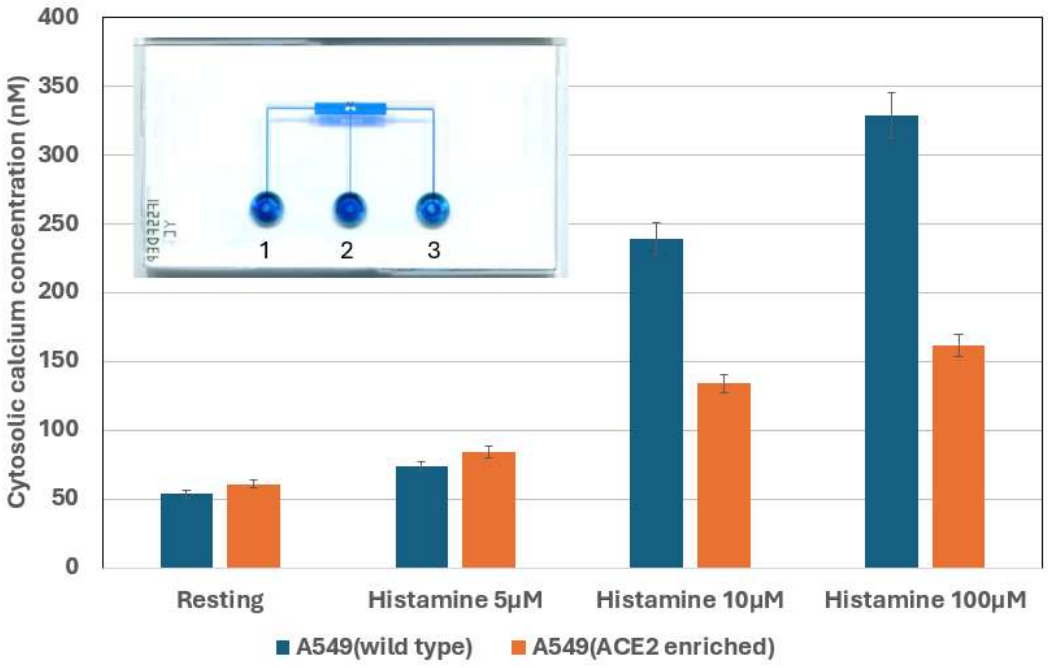


**Figure 6.** Comparison between cytosolic calcium concentration of wild type and ACE2-enriched A549 cells after the addition of different concentrations of histamine by single-cell analysis. Averages of three single-cell experiments are shown; the error bars represented the standard deviation of three measurements. An image of

 doi:10.20944/preprints202511.1437.v1



the microfluidic chip was included to depict the real-time data were collected using this single-cell chip. A typical real-time fluorescence curve for a single wild-type A549 cell is provided in Figure 5.

The changes of cytosolic calcium due to histamine are also measured in ACE2-enriched A549 cells, see Figure 6, which shows the concentrations of cytosolic calcium in single wild-type (blue) and ACE2-enriched A549 cells (orange). After adding different concentrations of histamine from 5 μM to 100 μM to the cells, there are increases in $[Ca^{2+}]_i$. The increase in the cytosolic calcium concentration of wild-type A549 cells is greater than those of ACE2-enriched A549 cells. As compared to ACE2-enriched cells, the wild type A549 has a lower resting level of calcium, but its increase after the addition of histamine is more intense, i.e., for 100 μM histamine, an increase of 6.5-fold (wild type) vs. 2.6-fold (ACE2) was observed. The greater increases in the wild-type A549 cells may be caused by physical or biochemical reasons; while the physical reason may be more histamine receptors in the unaltered wild-type cells, the biochemical reason is probably the absence of interactions of histamine and ACE2 receptors, which are both GPCRs [28,43].

Figure 7 illustrates the changes in the concentration of cytosolic calcium measured by bulk cell analysis of wild-type and ACE2-enriched A549 cells. The same pattern of cytosolic calcium increases in A549 cells in response to histamine stimulation compared to that of ACE2-enriched cells is observed. This observation strengthens the notion that ACE2-enrichment on A549 cells results in smaller response as compared to wild-type A549 cells.

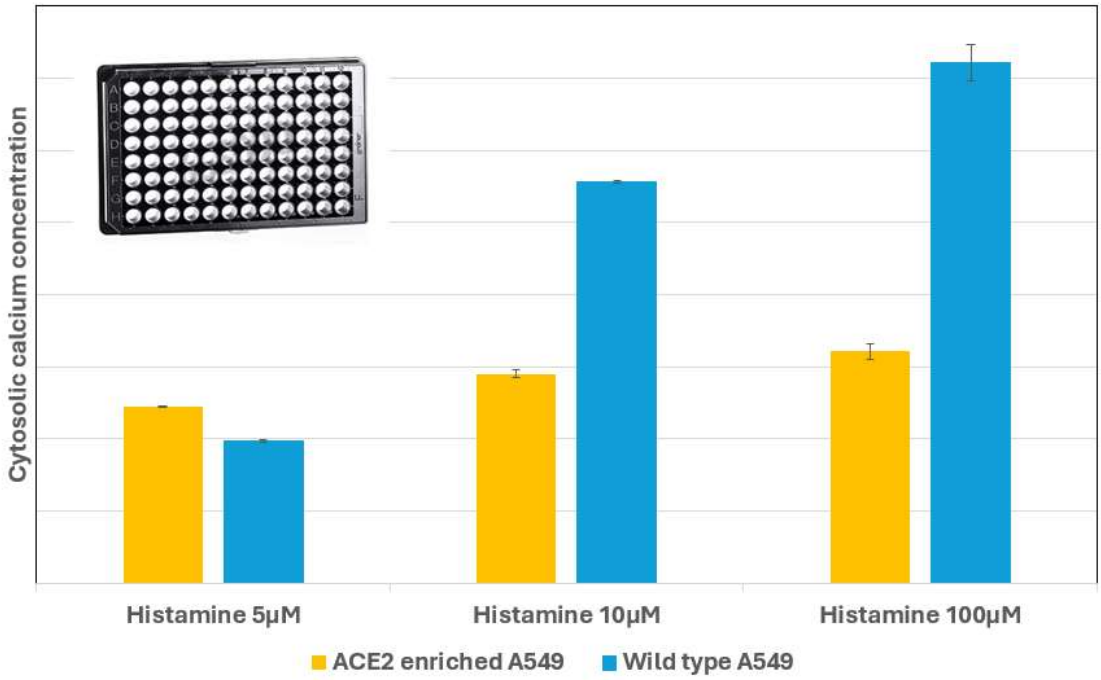


**Figure 7.** Bulk analysis of cytosolic calcium concentration of ACE2-enriched A549 cells and wild type A549 cells stimulated by different concentrations of histamine (n = 3). An image of the 96-well microplate was included to depict the data were collected using this bulk-cell measurement apparatus. The resting level, which was provided by the background of the cell-free well, was lower than the bars depicted for 5 μM histamine.

A direct comparison of the total cells, reagents (histamine and ionomycin) used is shown in Table 1. This comparison study confirms the results obtained from the bulk-cell measurements to be as good as those from the single-cell monitoring. While the bulk-cell measurements is an established method, it uses more reagents, i.e., 20 μL of 10X reagent in each well vs. 1 μL of 1X reagent in the microchip. For instance, for 10 μM ionomycin used to treat the cells in order to obtain Fmax, 20 μL of

 doi:10.20944/preprints202511.1437.v1



100 μM was used in each microplate well, but only 1 μL of 10 μM ionomycin was needed in each single-cell experiment, see Table 1.

**Table 1.** Comparison of the single-cell monitoring and bulk-cell measurements for cell calcium.

| | Cell number | Figure 6/7 | Reagent per conc. | Total cells | Total histamine | ionomycin |
|---|---|---|---|---|---|---|
| Single-cell | 100 in 1 μL per chip | 3 chip expts for wt and 3 for ACE | 100 μM in 1 μL = 0.1 nmol | 100 x 3 for wt and 300 for ACE | 0.69 nmol | 0.06 nmol |
| Bulk-cell | 10,000 in 200 μL per well | 9 wells for wt (3 reagent conc,) and 9 wells for ACE | 1000 μM in 20 μL = 20 nmol | 9 x 10,000 for wt and 90,000 for ACE | 414 nmol | 36 nmol |

For histamine, (0.005+0.01+0.1) x 6 = 0.69 nmol and (1+2+20) x 18 = 414 nmol. For ionomycin, 10 μM x 1 μL x 6 = 0.06 nmol and 100 μM x 20 μL x 18 = 36 nmol.

This high-throughput need has been achieved using droplet microfluidics in which thousands of cells are studied in thousands of nano-sized droplets. Furthermore, the issue of cell heterogeneity may be dealt with by obtaining cell information of thousands of cells in one experiment.

For instance, the droplet-based microfluidic device has allowed the investigations of thousands of individual cellular interactions in natural killer cells [44], of cytokine secretions/ immune interactions in single T cells [45,46], of exosome secretion/ drug interaction patterns of single tumor cells [47,48]. Such high throughput microfluidic methods have been used for single-cell transcriptome studies as well [49,50].

Heterogeneity has also been shown using droplet microfluidics for human cells [44,45], and also for bacteria, such as *P. aeruginosa* and *S. aureus* [51], or *E. coli* [52,53], or fungal pathogenicity on humans *C. albicans* [54].

## 4. Conclusions

The single-cell approach measures the calcium response in a single cell upon treatment with three concentrations of histamine. This method provides the temporal information for the cell to generate a calcium response upon reagent treatment, and the change of that response with time progression. However, our microchip method lacks the sample throughput to measure more cells, and the ability to detect the cell heterogeneity present in a cell population. In contrast, the bulk-cell calcium measurement approach offers the average cellular responses by analyzing a population of cells collectively. This approach measures more cells and allows researchers to understand the collective cell calcium response. Our two approaches do provide the cellular responses upon the reagent of several concentrations, though not the behaviors of individual cells in a heterogeneous cell population. Recent advances in microfluidic methods do address and overcome these limitations.

In our case, when cells and reagents are sufficient, the bulk-cell measurement approach is a well-established high-throughput method. But when both materials are limited, the single-cell approach provides an alternative way to obtain results, and even a better way to obtain cellular response of a reagent on the same single cell, which is not obscured by the average results generated by the bulk-cell measurements.

Furthermore, both approaches yielded consistent histamine-induced calcium responses, i.e., the wild-type A549 cells exhibited stronger responses than ACE2-enriched cells. The consistent results obtained by the two methods may well suggest a reason for the difference, perhaps due to a physical reason (more histamine receptors in the unaltered wild-type cells) or a biochemical reason (no competitive interactions of histamine with any ACE2 receptors).

 doi:10.20944/preprints202511.1437.v1



**Acknowledgments:** We are thankful to the financial support from Natural Sciences and Engineering Research Council (NSERC) of Canada.

## References

1. J. Liao, D. Patel, Q. Zhao, R. Peng, H. Guo, Z. Diwu, A Novel Ca2+ Indicator for Long-term Tracking of Intracellular Calcium Flux, BioTechniques 70 (2021) 271-277. https://doi.org/10.2144/btn-2020-0161
2. J. P. Robinson, R. Ostafe, S. N. Iyengar, B. Rajwa, R. Fischer, Flow Cytometry: The Next Revolution, Cells 12 (2023) 1875. https://doi.org/10.3390/cells12141875
3. K. Pang, S. Dong, Y. Zhu, X. Zhu, Q. Zhou, B. Gu, W. Jin, R. Zhang, Y. Fu, B. Yu, D. Sun, Z. Duanmu, X. Wei, Advanced flow cytometry for biomedical applications, J Biophotonics 16 (2023) e202300135. https://doi.org/10.1002/jbio.202300135
4. C. Ulbricht, R. Leben, A. Rakhymzhan, F. Kirchhoff , L. Nitschke, H. Radbruch, R. A Niesner, A. E. Hauser, Intravital quantification reveals dynamic calcium concentration changes across B cell differentiation stages, eLife 10 (2021) e56020. https://doi.org/10.7554/eLife.56020
5. A. R. Wheeler, W. R. Throndset, R. J. Whelan, A. M. Leach, R.N. Zare, Y. H. Liao, K. Farrell, I. D. Manger, A. Daridon, Microfluidic device for single-cell analysis, Anal. Chem. 2003, 75, 14, 3581–3586. https://doi.org/10.1021/ac0340758
6. Hamideh Sharifi Noghabi, Abdul Q. Ahmed, and Paul C. H. Li. Intracellular Calcium Increases due to Curcumin Measured using a Single-Cell Biochip. Anal. Lett.54 (2021) 2769-2776.
7. P Chen, X Feng, D Chen, C Liu, W Du, BF Liu, Investigating intercellular calcium waves by microfluidic gated pinched-flow, Sens. Actuat. B 234 (2016) 583-592. https://doi.org/10.1016/j.snb.2016.04.184
8. T Xu, W Yue, CW Li, X Yao, M Yang, Microfluidics study of intracellular calcium response to mechanical stimulation on single suspension cells, Lab Chip, 13 (2013) 1060-1069. https://doi.org/10.1039/c3lc40880a
9. S Faley, K Seale, J Hughey, DK Schaffer, S. Van Compernolle, B. McKinney, F. Baudenbacher, D. Unutmaze, J. P. Wikswo, Microfluidic platform for real-time signaling analysis of multiple single T cells in parallel, Lab Chip, 8 (2008) 1700–1712. https://doi.org/10.1039/b719799c
10. XiuJun Li, Paul C.H. Li, Strategies for the real-time detection of calcium channel events of single cells: recent advances and new possibilities. Expert Review of Clinical Pharmacology, 3 (2010) 267-280.
11. A. Takahashi, P. Camacho, J.D. Lechleiter, B. Herman, Measurement of Intracellular Calcium, Physiological Reviews. 79 (1999) 1089–1125. https://doi.org/10.1152/physrev.1999.79.4.1089.
12. A.S. Hauser, M.M. Attwood, M. Rask-Andersen, H.B. Schiöth, D.E. Gloriam, Trends in GPCR drug discovery: new agents, targets and indications, Nat Rev Drug Discov. 16 (2017) 829–842. https://doi.org/10.1038/nrd.2017.178.
13. S. Martewicz , F. Michielin , E. Serena , A. Zambon , M. Mongillo , N. Elvassore, Reversible alteration of calcium dynamics in cardiomyocytes during acute hypoxia transient in a microfluidic platform, Integr. Biol. 4 (2012) 153–164. https://doi.org/10.1039/c1ib00087j
14. X.J. Li, P.C.H. Li, Microfluidic selection and retention of a single cardiac myocyte, on-chip dye loading, cell contraction by chemical stimulation, and quantitative fluorescent analysis of intracellular calcium, Anal. Chem., 77 (2005) 4315-4322.
15. S. Kou, L. Pan, D. van Noort, G Meng, X. Wu, H. Sun, J. Xu, I. Lee, A multishear microfluidic device for quantitative analysis of calcium dynamics in osteoblasts, Biochem. Biophy. Res. Comm. 408 (2011) 350-355. https://doi.org/10.1016/j.bbrc.2011.04.044
16. A. Rahimi, H. Sharifi, P.C.H. Li, Cytosolic Calcium Measurement Utilizing a Single-Cell Biochip to Study the Effect of Curcumin and Resveratrol on a Single Glioma Cell, Methods Mol Biol. 2689 (2023) 13–25. https://doi.org/10.1007/978-1-0716-3323-6_2.
17. A Lopez-Canosa, S Perez-Amodio, E Engel, O. Castaño, Microfluidic 3D platform to evaluate endothelial progenitor cell recruitment by bioactive materials, Acta Biomaterialia, 151 (2022) 264-277. https://doi.org/10.1016/j.actbio.2022.08.019
18. C Huang, Q Ramadan, JB Wacker, HC Tekin, C Ruffert, G Vergeres, P Silacci, MAM Gijs, Microfluidic chip for monitoring Ca2+ transport through a confluent layer of intestinal cells, RSC Adv. 4(2014) 52887. https://doi.org/10.1039/c4ra09370d

 doi:10.20944/preprints202511.1437.v1




19. ZZ Chen, WM Yuan, C Xiang, DP Zeng, B Liu, K R Qin, A microfluidic device with spatiotemporal wall shear stress and ATP signals to investigate the intracellular calcium dynamics in vascular en-dothelial cells, Biomech Model Mechanobiol 18 (2019) 189–202. https://doi.org/10.1007/s10237-018-1076-x
20. A Jovic, SM Wade, RR Neubig, JJ Linderman, S Takayama, Microfluidic interrogation and mathematical modeling of multi-regime calcium signaling dynamics, Integr. Biol. 5 (2013) 932–939. https://doi.org/10.1039/c3ib40032h
21. S Feng, Q Zhang, T Xie, Y Hou, JM Lin, In-situ monitoring calcium signaling through tumor microtubes for single cell-cell communication via an open microfluidic probe, Biosens. Bioe-lect. 206 (2022) 114137. https://doi.org/10.1016/j.bios.2022.114137
22. X Zhang, H Yin, JM Cooper, SJ Haswell, A microfluidic-based system for analysis of sin-gle cells based on Ca2+ flux, Electrophoresis, 27 (2006) 5093-5100. https://doi.org/10.1002/elps.200600390
23. K. Manohar, R.K. Gupta, P. Gupta, D. Saha, S. Gare, R. Sarkar, A. Misra, L. Giri, FDA approved L-type channel blocker Nifedipine reduces cell death in hypoxic A549 cells through modulation of mitochondrial calcium and superoxide generation, Free Radic Biol Med. 177 (2021) 189–200. https://doi.org/10.1016/j.freeradbiomed.2021.08.245.
24. H.-J. Kim, P.C.W. Lee, J.H. Hong, Lamin-A/C Is Modulated by the Involvement of Hista-mine-Mediated Calcium/Calmodulin-Dependent Kinase II in Lung Cancer Cells, Int J Mol Sci. 23 (2022) 9075. https://doi.org/10.3390/ijms23169075.
25. J. Paltauf-Doburzynska, M. Frieden, M. Spitaler, W.F. Graier, Histamine-induced Ca2+ oscilla-tions in a human endothelial cell line depend on transmembrane ion flux, ryanodine receptors and endoplasmic reticulum Ca2+-ATPase, J Physiol. 524 (2000) 701–713. https://doi.org/10.1111/j.1469-7793.2000.00701.x
26. C.D. Zappia, G. Granja-Galeano, N. Fernández, C. Shayo, C. Davio, C.P. Fitzsimons, F. Monczor, Effects of histamine H1 receptor signaling on glucocorticoid receptor activity. Role of ca-nonical and non-canonical pathways, Sci Rep. 5 (2015) 17476. https://doi.org/10.1038/srep17476.
27. W.-C. Huang, C.-Y. Chai, W.-C. Chen, M.-F. Hou, Y.-S. Wang, Y.-C. Chiu, S.-R. Lu, W.-C. Chang, S.-H.H. Juo, J.-Y. Wang, W.-C. Chang, Histamine regulates cyclooxygenase 2 gene activa-tion through Orai1-mediated NFκB activation in lung cancer cells, Cell Calcium. 50 (2011) 27–35. https://doi.org/10.1016/j.ceca.2011.04.004.
28. C.P. Fitzsimons, F. Monczor, N. Fernández, C. Shayo, C. Davio, Mepyramine, a histamine H1 receptor inverse agonist, binds preferentially to a G protein-coupled form of the receptor and se-questers G protein, J Biol Chem. 279 (2004) 34431–34439. https://doi.org/10.1074/jbc.M400738200.
29. X.J. Li, J. Huang, G.F. Tibbits, P.C.H. Li, Real-time monitoring of intracellular calcium dynamic mobilization of a single cardiomyocyte in a microfluidic chip pertaining to drug discovery, Electro-phoresis, 28 (2007) 4723-4733.
30. S.T. Holgate, The epithelium takes centre stage in asthma and atopic dermatitis, Trends Immunol. 28 (2007) 248–251. https://doi.org/10.1016/j.it.2007.04.007.
31. T. Liu, L. Zhang, D. Joo, S.-C. Sun, NF-κB signaling in inflammation, Signal Transduct Target Ther. 2 (2017) 17023-. https://doi.org/10.1038/sigtrans.2017.23.
32. S. Smolinska, M. Jutel, R. Crameri, L. O'Mahony, Histamine and gut mucosal immune regulation, Allergy. 69 (2014) 273–281. https://doi.org/10.1111/all.12330.
33. M. Jutel, K. Blaser, C.A. Akdis, Histamine in allergic inflammation and immune modulation, Int Arch Allergy Immunol. 137 (2005) 82–92. https://doi.org/10.1159/000085108.
34. M.M. Thakkar, Histamine in the regulation of wakefulness, Sleep Med Rev. 15 (2011) 65–74. https://doi.org/10.1016/j.smrv.2010.06.004.
35. W.-K. Cai, J. Hu, T. Li, J.-R. Meng, X. Ma, S.-J. Yin, C.-H. Zhao, G.-H. He, G.-L. Xu, Activation of histamine H4 receptors decreases epithelial-to-mesenchymal transition progress by inhibiting transforming growth factor-β1 signalling pathway in non-small cell lung cancer, Eur J Cancer. 50 (2014) 1195–1206. https://doi.org/10.1016/j.ejca.2013.12.025.
36. C.-W. Chang, K.M. Parsi, M. Somasundaran, E. Vanderleeden, P. Liu, J. Cruz, A. Cousineau, R.W. Finberg, E.A. Kurt-Jones, A Newly Engineered A549 Cell Line Expressing ACE2 and TMPRSS2 Is Highly Permissive

 doi:10.20944/preprints202511.1437.v1



to SARS-CoV-2, Including the Delta and Omicron Variants, Viruses. 14 (2022) 1369. https://doi.org/10.3390/v14071369.

37. X. Li, X. Xue, P.C.H. Li, Real-time detection of the early event of cytotoxicity of herbal ingredients on single leukemia cells studied in a microfluidic biochip, Integr. Biol. 1 (2009) 90–98. https://doi.org/10.1039/B812987H.
38. Gee, K. R., K. A. Brown, W. N. U. Chen, J. Bishop-Stewart, D. Gray, and I. Johnson. Chemical and physiological characterization of Fluo-4 Ca2+-indicator dyes. Cell Calcium. 27 (2000) 97–106. doi:10.1054/ceca.1999.0095.
39. P.L. Nguyen, Pathophysiological Roles of Histamine Receptors in Cancer Progression: Implica-tions and Perspectives as Potential Molecular Targets, Biomolecules. 11 (2021) 1232. https://doi.org/10.3390/biom11081232.
40. Y. Jiang, H. Li, Y. Wang, T. Tian, Y. He, Y. Jin, C. Han, X. Jin, F. Zhang, E. Morii, ALDH enzyme activity is regulated by Nodal and histamine in the A549 cell line, Oncol Lett. 14 (2017) 6955–6961. https://doi.org/10.3892/ol.2017.7057.
41. S. Hou, S.H. Heinemann, T. Hoshi, Modulation of BKCa channel gating by endogenous signaling molecules, Physiology (Bethesda). 24 (2009) 26–35. https://doi.org/10.1152/physiol.00032.2008.
42. E.E. Benarroch, Chapter 8 - Neurotransmitters, in: S.A. Waldman, A. Terzic (Eds.), Pharmacol-ogy and Therapeutics: principles to practice, W.B. Saunders, Philadelphia, 2009: pp. 91–113. https://doi.org/10.1016/B978-1-4160-3291-5.50012-3.
43. M.O. Lonchampt, P. Marche, C. Demerle, A. Girard, M. Cabanie, A. Esanu, P.E. Chabrier, P. Braquet, Histamine H1-receptors mediate phosphoinositide and calcium response in cultured smooth muscle cells-interaction with cicletanine (CIC), Agents and Actions. 24 (1988) 255–260. https://doi.org/10.1007/BF02028280.
44. Subedi, N., Van Eyndhoven, L.C., Hokke, A.M. et al. An automated real-time microfluidic platform to probe single NK cell heterogeneity and cytotoxicity on-chip. Sci Rep 11, 17084 (2021). https://doi.org/10.1038/s41598-021-96609-9. https://doi.org/10.1038/s41598-021-96609-9
45. R. Dimatteo and D. Di Carlo, IL-2 secretion-based sorting of single T cells using high-throughput microfluidic on-cell cytokine capture. Lab Chip, 2022, 22, 1576 DOI: 10.1039/D1LC01098K
46. Sullivan, M.R., Ugolini, G.S., Sarkar, S. et al. Quantifying the efficacy of checkpoint inhibitors on CD8+ cytotoxic T cells for immunotherapeutic applications via single-cell interaction. Cell Death Dis 11, 979 (2020). https://doi.org/10.1038/s41419-020-03173-7
47. Fangteng Song, Chao Wang, Chunhua Wang, Jianbo Wang, Yu Wu, Yihe Wang, Hong Liu, Yu Zhang, Lin Han. Multi-Phenotypic Exosome Secretion Profiling Microfluidic Platform for Exploring Single-Cell Heterogeneity. Small Methods, 2022, 6 (9), 2200717. https://doi.org/10.1002/smtd.202200717
48. S. Sarkar, N. Cohen, P. Sabhachandani and T. Konry. Phenotypic drug profiling in droplet microfluidics for better targeting of drug-resistant tumors. Lab Chip, 2015,15, 4441-4450 https://doi.org/10.1039/C5LC00923E
49. Sagar N. Agnihotri, Giovanni Stefano Ugolini, Matthew Ryan Sullivan, Yichao Yang, Augustin de Ganzo, Ji Won Lim, Tania Konry. Droplet Microfluidics for Functional Temporal Analysis and Cell Recovery on Demand using Microvalves: Application in Immunotherapies for Cancer Lab Chip, 2022,22, 3258-3267. https://doi.org/10.1039/D2LC00435F
50. Langerman, J., Baghdasarian, S., Cheng, R.YH. et al. Linking single-cell transcriptomes with secretion using SEC-seq. Nat Protoc 20, 2034–2055 (2025). https://doi.org/10.1038/s41596-024-01112-w
51. N. Pacocha, M. Zapotoczna, K. Makuch, J. Bogusławski and P. Garstecki, You will know by its tail: a method for quantification of heterogeneity of bacterial populations using single-cell MIC pro-filing. Lab Chip, 2022, 22, 4317. https://doi.org/10.1039/D2LC00234E
52. Giampaolo Pitruzzello, Christoph G. Baumann, Steven Johnson, Thomas F. Krauss. Single-Cell Motility Rapidly Quantifying Heteroresistance in Populations of Escherichia coli and Salmonella typhimurium. Small Science. 2022, 2(5), 2100123. https://doi.org/10.1002/smsc.202100123
53. Sagar N. Agnihotri, Nikos Fatsis-Kavalopoulos, Jonas Windhager, Maria Tenje, Dan I. Andersson. Droplet microfluidics–based detection of rare antibiotic-resistant subpopulations in Escherichia coli from

 doi:10.20944/preprints202511.1437.v1



bloodstream infections. Sci. Adv. 11, eadv4558 (2025) https://www.science.org/doi/full/10.1126/sciadv.adv4558

54. Lukasz Kozubowski, Judith Berman, The impact of phenotypic heterogeneity on fungal patho-genicity and drug resistance, FEMS Microbiology Reviews, 2025, 49, fu-af001, https://doi.org/10.1093/femsre/fuaf001